Supporting Information

Multifunctional MXene-based Composites Film with Simultaneous Terahertz/Gigahertz Wave Shielding Performance for Future 6G Communication

Zheng Cheng[a], Yishu Cao[a], Ruofeng Wang[a], Xiaoyan Liu[a], Fei Fan[b], Yi Huang*[a]

a National Institute for Advanced Materials, Tianjin Key Laboratory of Metal and Molecule Based Material Chemistry, Key Laboratory of Functional Polymer Materials, Collaborative Innovation Center of Chemical Science and Engineering (Tianjin), School of Materials Science and Engineering, Nankai University, Tianjin, 300350, China

b Institute of Modern Optics, Nankai University, Tianjin Key Laboratory of Micro-scale Optical Information Science and Technology, Tianjin 300350, PR China

*Corresponding author: yihuang@nankai.edu.cn (Professor Yi Huang)

1 Hydrogen-bonding interactions between PA and MXene sheet from IR Results

Figure S2a displayed the IR spectra of M/A films and pure MXene. Compared with the pure PA film (M/A-0), significant changes could be observed for M/A films at 1251cm^{-1} (Figure S2b) and 1655cm^{-1} (Figure S2c), which are attributed to C-N and C=O stretching of NHCO from PA. It is believed that high-density hydrogen bonding interactions were generated between H atoms from NHCO and O/F atoms from MXene surface, thus inducing such changes in these NHCO-related peaks.

2 Thickness effects on the THz shielding performance of M/A films

The results in Figure S7a indicates that transmission signals get obviously weakened with a higher thickness (40μm), while their reflection signals maintain stable (Figure S7b). Besides, their calculated THz shielding efficiency results (Figure S7c/d) are rather different, and a 40μm film shows an average SE value of 51.2dB, much higher than the 38.7dB of 20μm film. The SE_R and SE_A results explains that their SE_R values are rather similar, with a low value of nearly 5dB, while their SE_a values are improved with the film thickness. Therefore, we can draw a safe conclusion that a high thickness of films

would enhance the absorption ratio for THz waves, and generates a better shielding efficiency in THz band.

3 Detail permittivity and permeability of composite film composite films

Figure S8 presents the permittivity and permeability of composite film in X band. It is seen that the original M/A-0 film displayed low ε′ and ε″ value (Figure S8a/b), which are both lower than 10 in X band. This is resulted from the weak dielectric loss properties which comes from the dipolar polarization of those polar groups (NHCO, benzimidazole etc.). With the incorporation of MXene sheets, the permittivity of composite films is increasing, with several orders of magnitude growth. The large improvements of ε′ and ε″ values are attributed to the high conductivity of MXene sheets. As reported by many literatures[1, 2], $Ti_3C_2X_n$ demonstrates the metallic nature of their conductivities, with high free carrier density (up to $8 \pm 3 \times 10^{21}$ cm^{-3}) and mobility (up to 0.7 ± 0.2 cm^2/V s), and this endows the composite films with improved ε′ and ε″ values. While for the permeability, the corresponding values of them (u′ and u″ in Figure S8c/d) don't change much with the incorporation of MXene sheets, and this is derived from the weak magnetic properties of both PA and MXene.

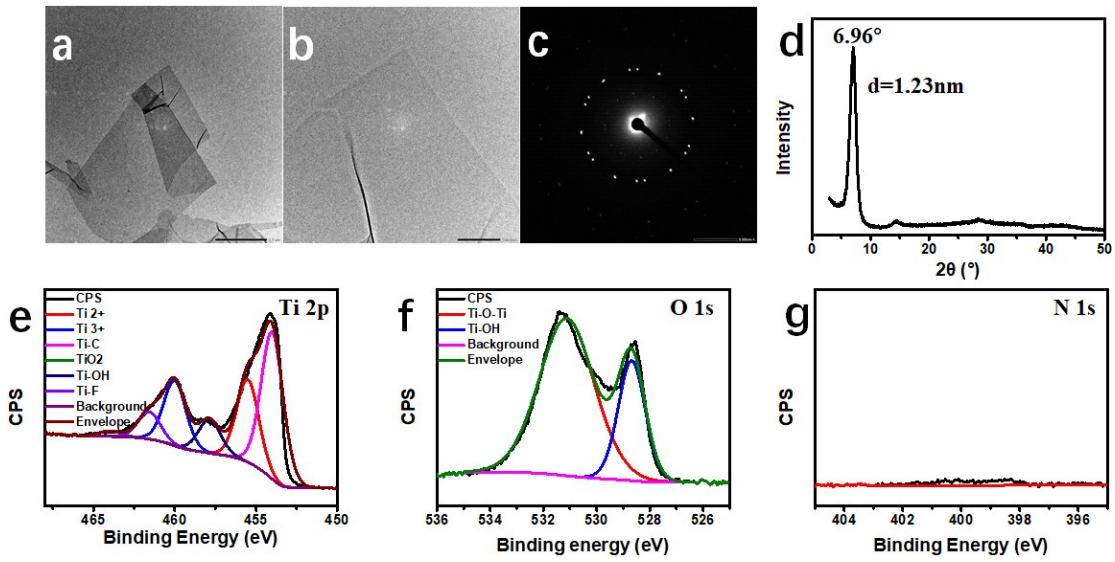

Figure S1 (a-c) TEM images and crystal diffraction of MXene sheet, (d) XRD of MXene, XPS Ti2p(e), O1s(e) and N1s (g) spectra of MXene sheet,

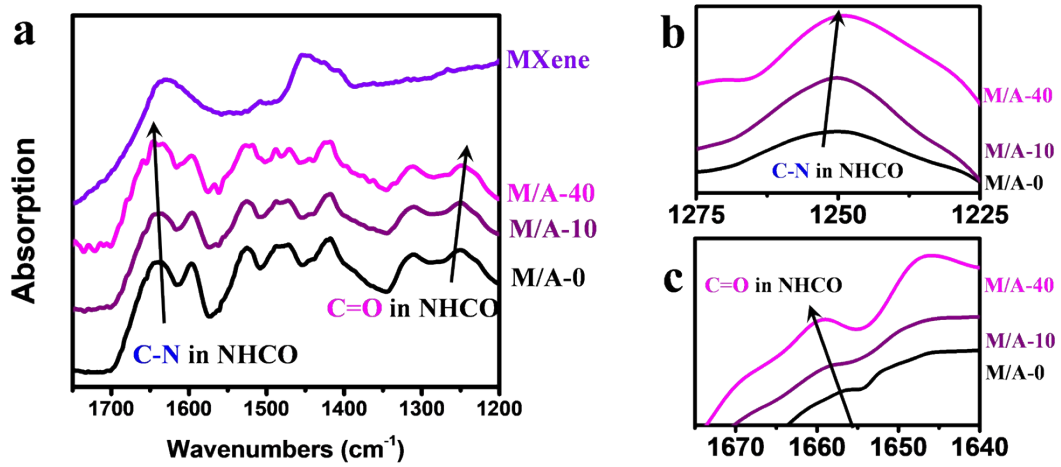

Figure S2 (a) IR spectra of MXene and M/A films, and corresponding enlargement at 1225-1275cm^{-1} (b) and 1640-1680cm^{-1} (c)

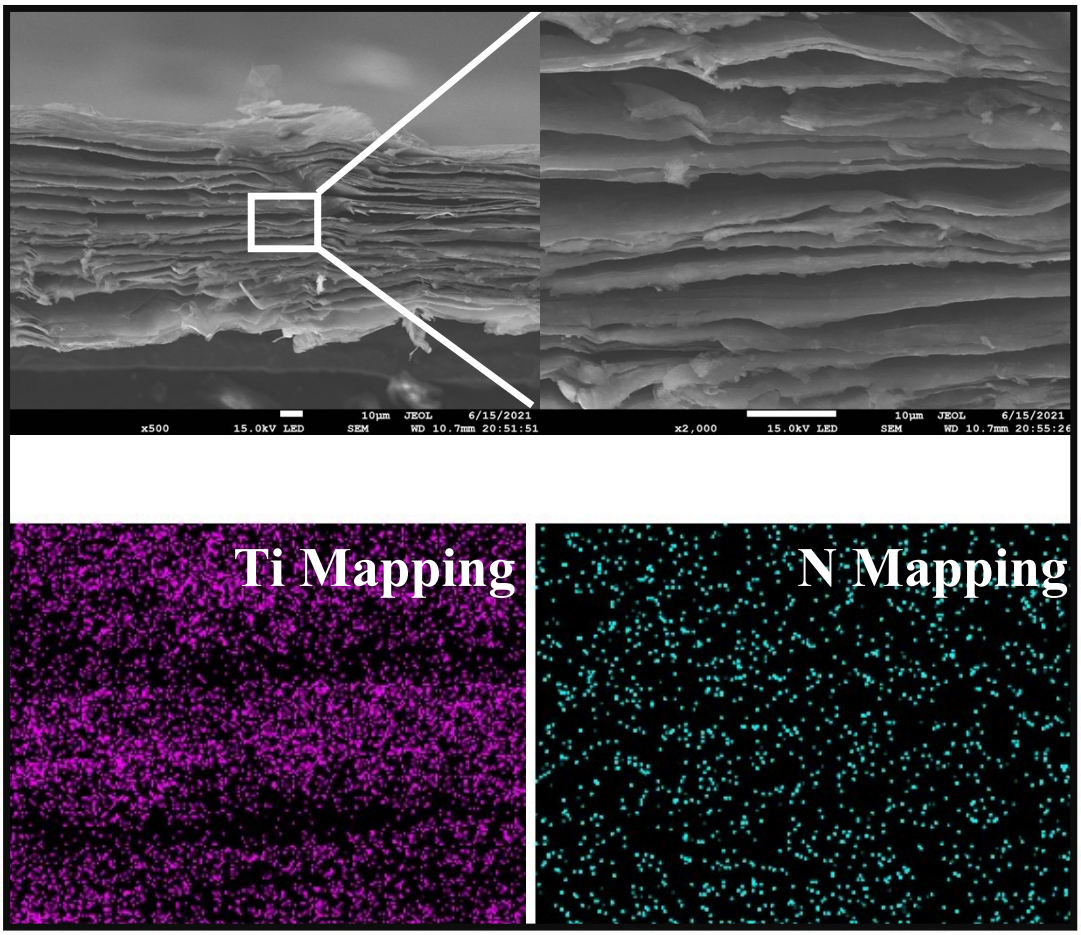

Figure S3 SEM and EDS mapping results of M/A-20

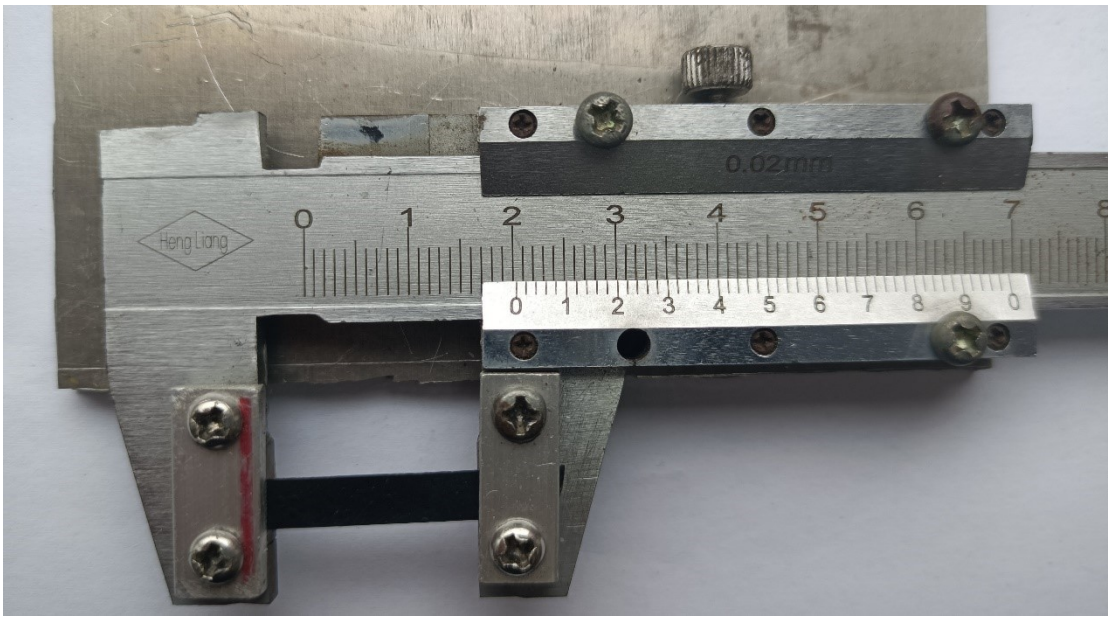

Figure S4 home-made devices for in-situ Raman test with different strains

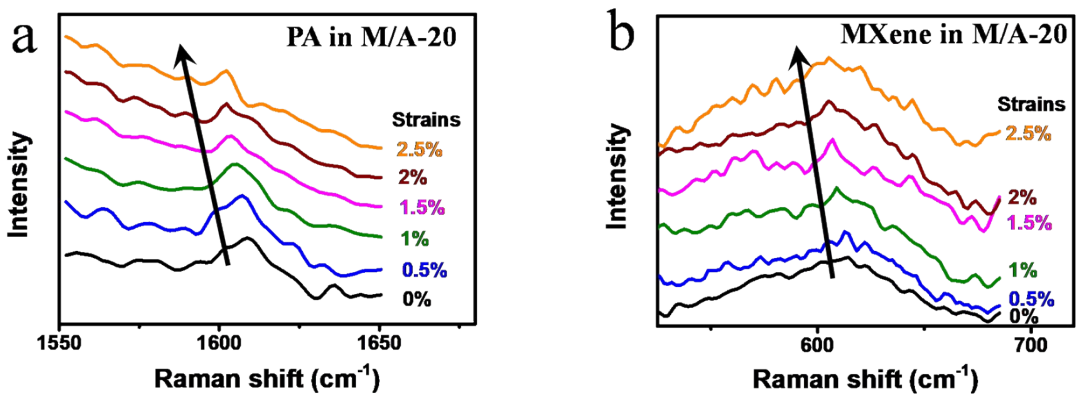

Figure S5 In-situ Raman test of composites films with different strains in 1550-1675cm^{-1} (a for PA in M/A-20) and 500-750cm^{-1} (b for MXene in M/A-20)

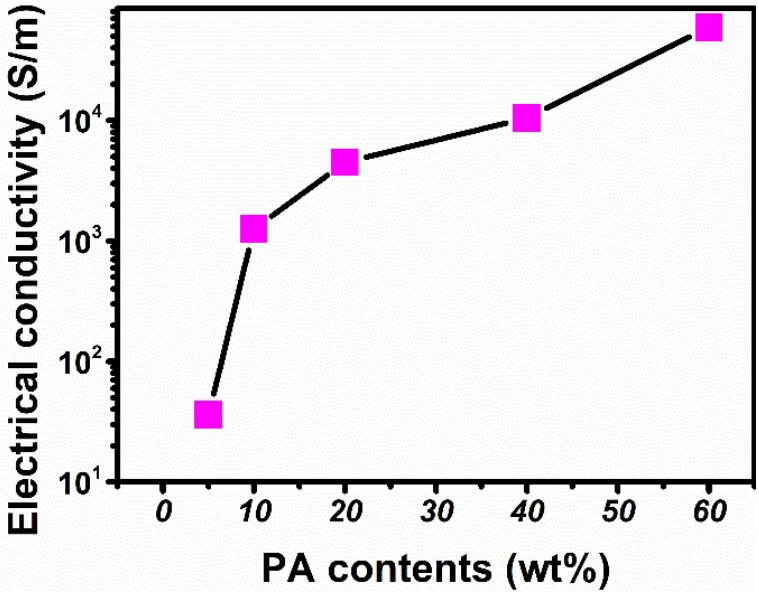

Figure S6 Electrical conductivity data of M/A films

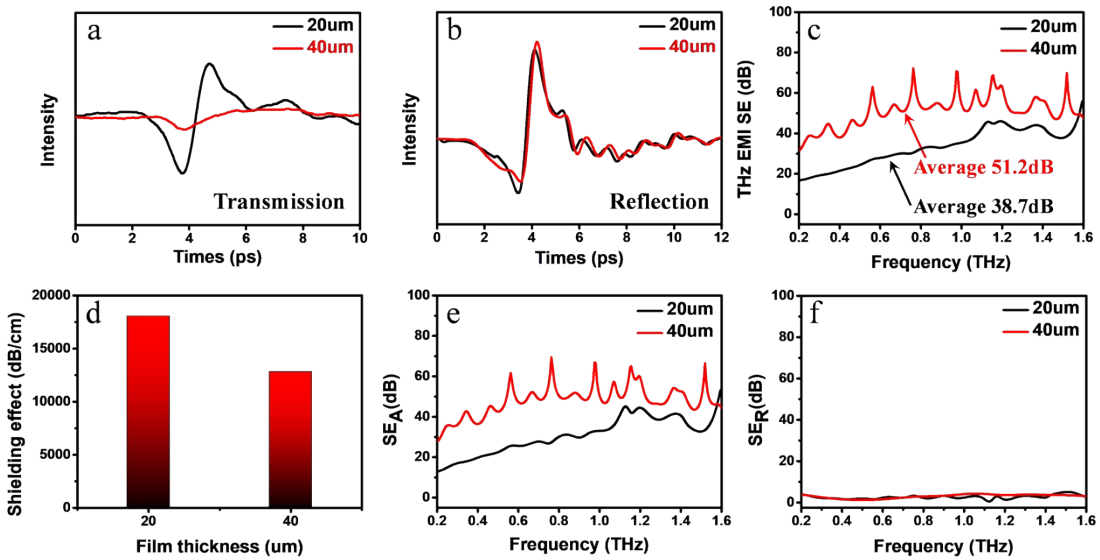

Figure S7 (a) Transmission and (b) Reflection signals of M/A-20 film with different thickness, (c) THz wave shielding effects in 0.2-1.6THz, (d) their average SE values per unit thickness, corresponding (e)SE_A and (f) SE_R results for film with different thickness

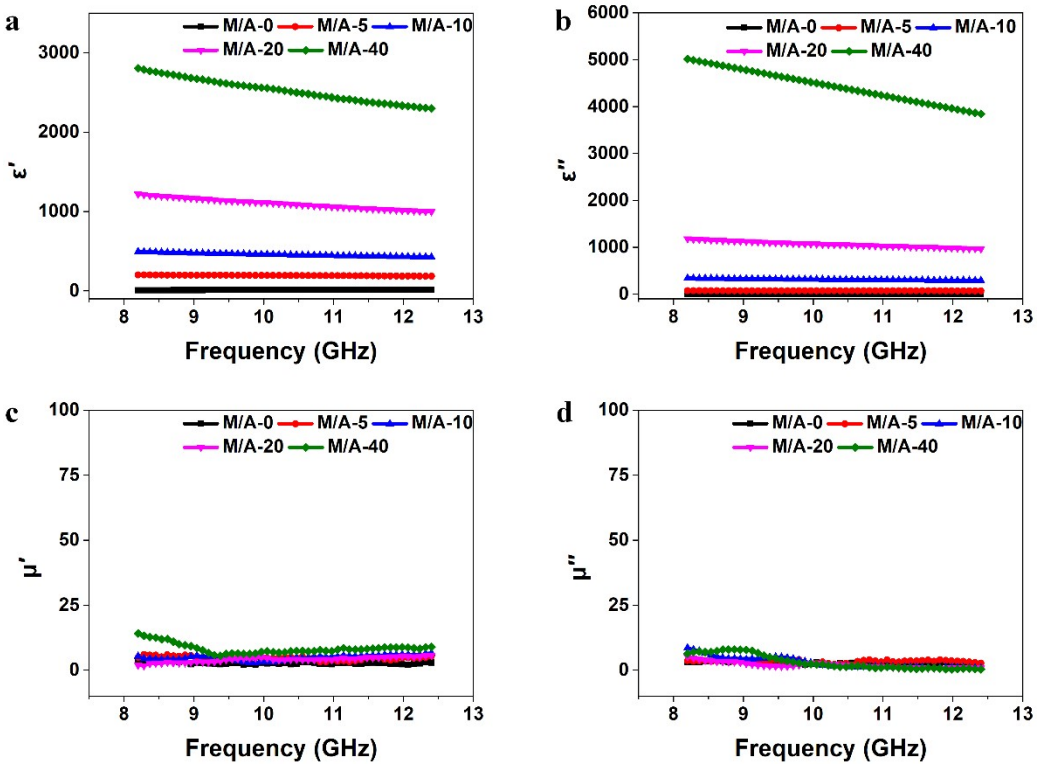

Figure S8 Real part (a) and imaginary part (b) of complex permittivity for M/A films; real part (c) and imaginary part (d) of complex permeability

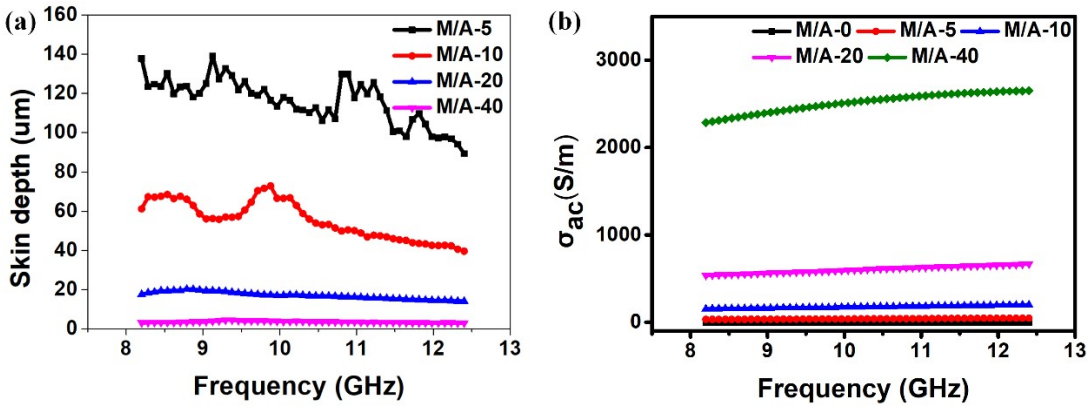

Figure S9 (a) Skin depth data of M/A films; (b) AC conductivity of M/A films

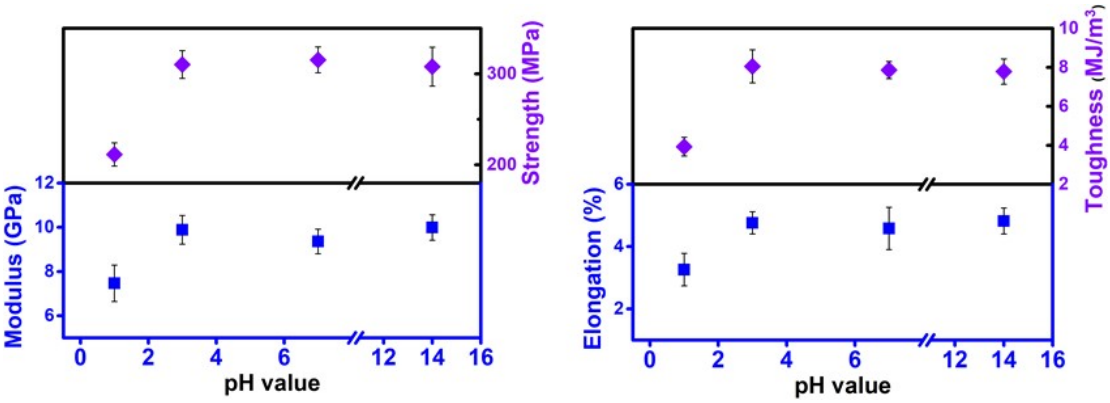

Figure S10 Summary of mechanical changes of M/A-20 with different PH solution treatments

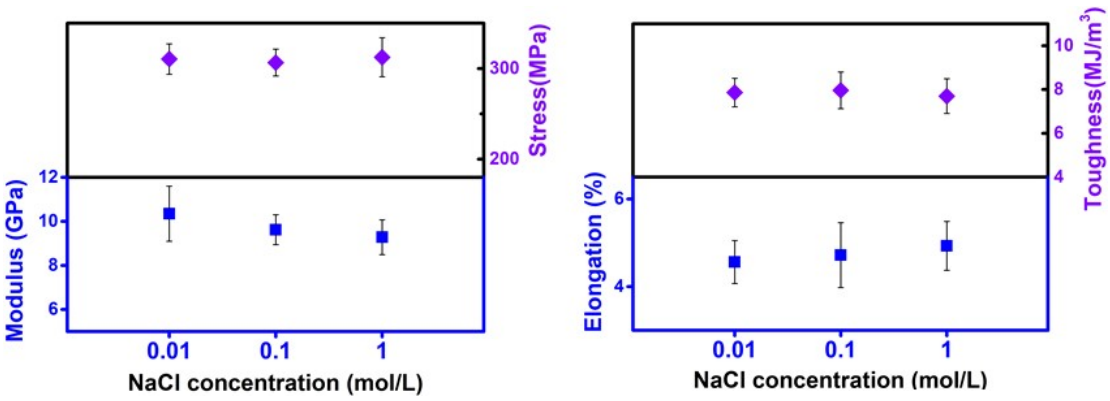

Figure S11 Summary of mechanical changes of M/A-20 with different NaCl solution treatments

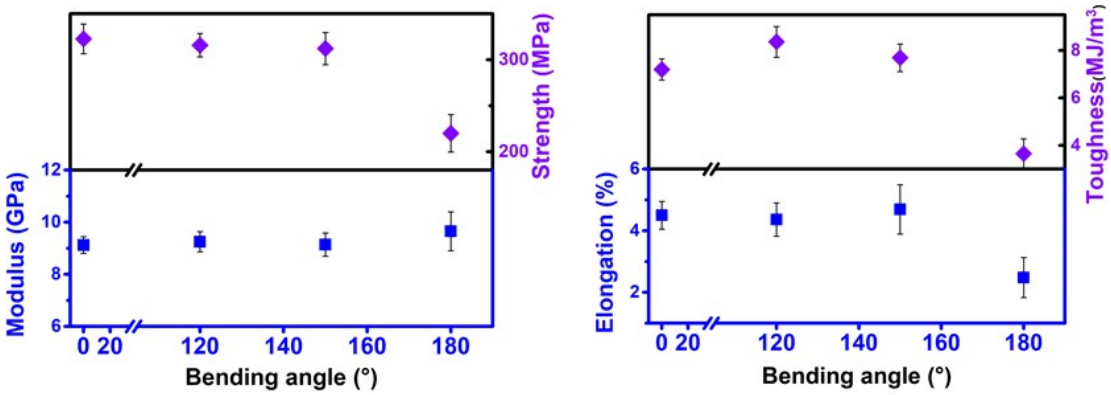

Figure S12 Summary of mechanical changes of M/A-20 subjected to 1000 times of bending with different bending angle

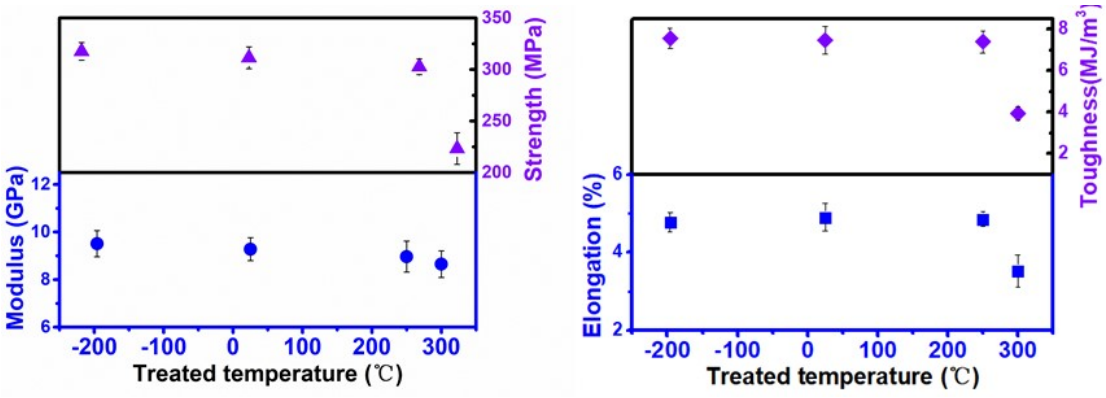

Figure S13 Summary of mechanical changes of M/A-20 with different temperature treatments

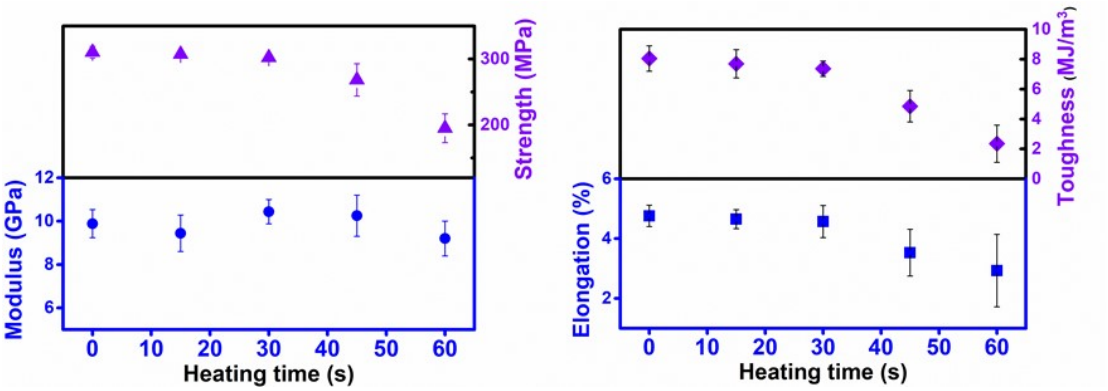

Figure S14 Summary of mechanical changes of M/A-20 treated in 500 ℃ environment with different times

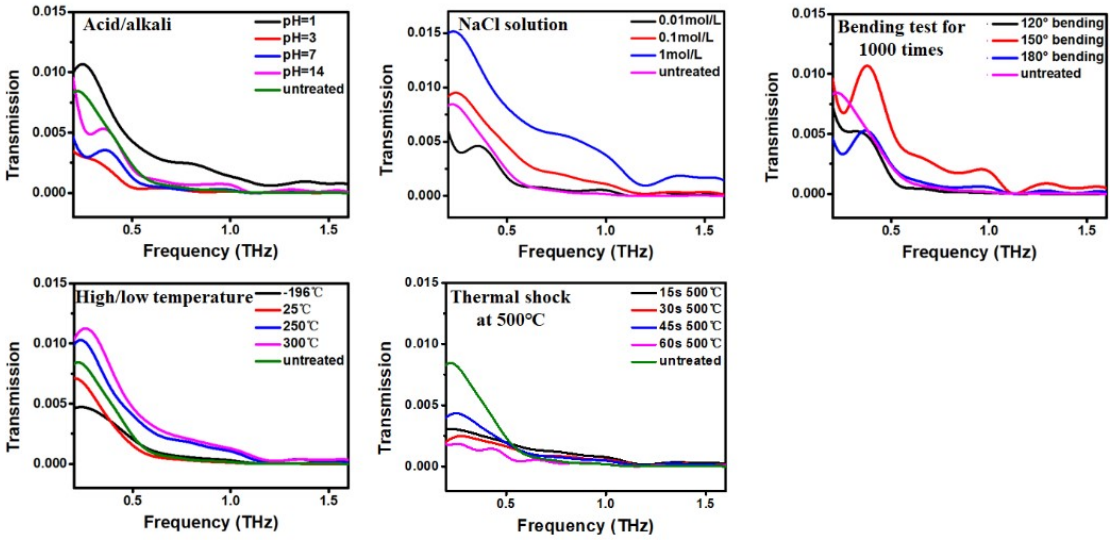

Figure S15 THz transmission of M/A-20 subjected to various harsh environment

Table S1: Comparison of highest joule-heating output temperatures of various MXene-based composites films

Film Type	Highest output temperature (°C)	Refs
MXene/montmorillonite film	141	[3]
PI Fiber/MXene film	105	[4]
MXene-Decorated Polyester Textiles	79	[5]
MXene-xanthan nanocomposite films	136.5	[6]
PAN@PPy/MXene film	170.6	[7]
MXene/Aramid Fiber film	146.1	[8]
CNTs@MXene/cellulose film	154	[9]
phase change capsules /MXene/PVA film	115	[10]
MXene/PA film	225	This work

References

1. A. Miranda, J. Halim, M. Barsoum and A. Lorke, *Applied Physics Letters*, 2016, **108**, 033102.
2. L. Zhou, Y. Zhang, Z. Zhuo, A. J. Neukirch and S. Tretiak, *The journal of physical chemistry letters*, 2018, **9**, 6915-6920.
3. L. Li, Y. Cao, X. Liu, J. Wang, Y. Yang and W. Wang, *ACS applied materials & interfaces*, 2020, **12**, 27350-27360.
4. K. Sun, F. Wang, W. Yang, H. Liu, C. Pan, Z. Guo, C. Liu and C. Shen, *ACS Applied Materials & Interfaces*, 2021, **13**, 50368-50380.
5. Q. W. Wang, H. B. Zhang, J. Liu, S. Zhao, X. Xie, L. Liu, R. Yang, N. Koratkar and Z. Z. Yu, *Advanced Functional Materials*, 2019, **29**, 1806819.
6. Y. Sun, R. Ding, S. Y. Hong, J. Lee, Y.-K. Seo, J.-D. Nam and J. Suhr, *Chemical Engineering Journal*, 2021, **410**, 128348.
7. F. Wu, Z. Tian, P. Hu, J. Tang, X. Xu, L. Pan, J. Liu, P. Zhang and Z. Sun, *Nanoscale*, 2022, **14**, 18133-18142.
8. J. Wang, X. Ma, J. Zhou, F. Du and C. Teng, *ACS nano*, 2022, **16**, 6700-6711.
9. Y. Zhang, W. Wang, J. Xie, K. Dai, F. Zhang and Q. Zheng, *Carbon*, 2022, **200**, 491-499.
10. S. Gong, X. Sheng, X. Li, M. Sheng, H. Wu, X. Lu and J. Qu, *Advanced Functional Materials*, 2022, 2200570.